ARTICLE

Check for updates

Journal of
Sensor Science and Technology

The Korean Sensors Society

Feedforward Countersignal Control to Suppress Magnetic Field Coupling in Electromagnetic 2D MEMS Scanners

Sang-Gyun Gi[1,*], Sehwan Park[1,*], Junseop Lee[1], Seungjoo Lee[1], and Jihyuk Cho[1,+]

[1]*IT Convergence System Research Center, Korea Electronics Technology Institute (KETI), 25, Saenari-ro, Bundang-gu, Seongnam-si, Gyeonggi-do, 13509, Republic of Korea*

Cite This: *J. Sens. Sci. Technol. Vol. 34, No. 6 (2025) 668-675*

https://doi.org/10.46670/JSST.2025.34.6.668

ABSTRACT: 2D MEMS mirrors are widely used in compact LiDAR systems for high-resolution raster scanning. However, magnetic field coupling induces crosstalk between resonant and linear (non-resonant) axes in electromagnetic 2D MEMS, which degrades scan linearity and positional accuracy. In this study, we propose a digital feedforward control scheme for electromagnetic 2D MEMS that uses a countersignal to suppress high-frequency inter-axis crosstalk. The control system synthesizes a countersignal that is proportional and phase-opposed to a counterpart driving signal. The countersignal is generated based on the experimentally measured system gains at the resonant frequency, and can be implemented efficiently on an FPGA without requiring feedback control or complex computational resources. The feasibility of the proposed approach was validated on an experimental setup comprising an FPGA platform, a 2D MEMS mirror, and drive electronics. The experimental results demonstrated significant improvements: the RMS and maximum errors of the linear axis decreased by 38% and 49%, respectively, while the coefficient of determination (R^2) increased from 0.991 to 0.996. In addition, the slope variation coefficient was reduced from 243% to 59%, which confirms the enhanced scanning uniformity. Overall, the proposed method offers a computationally efficient, scalable, and real-time solution for precise MEMS-based optical scanning in LiDAR and 3D imaging systems.

KEYWORDS: *MEMS, Raster scan, LiDAR, Crosstalk, Feedforward, Crosstalk-cancellation, FPGA implementation*

1. INTRODUCTION

Scanners based on mirrors comprising micro-electromechanical systems (MEMS) have been widely adopted in light detection and ranging (LiDAR) systems for compact and power-efficient beam steering [1-3]. In particular, two-dimensional (2D) MEMS mirrors enable high-resolution imaging with a wide field of view (FOV) through raster scanning [2], in which the resonant axis provides high-speed horizontal motion and the linear axis ensures precise scanning. This dual-axis operation enables real-time generation of dense raster patterns. Thus, MEMS mirrors are essential in miniaturized LiDAR systems.

However, 2D MEMS scanners often suffer from cross-axis coupling with specific causes that depend on the MEMS design. For example, electromagnetic actuation is primarily affected by magnetic field coupling [4,5], electrostatic actuation by electric field coupling [5], and piezoelectric actuation by mechanical stress/strain coupling [3,6,7], which can all lead to crosstalk that degrades scan linearity and positional accuracy [3,5] and ultimately distorts the scanning pattern of the point cloud [8]. These effects become more significant under high-speed operation.

Various mitigation strategies have been investigated to address these issues. For electromagnetic MEMS, structural mitigation techniques [9] have been reported to implement magnetic shielding and optimize coil geometries to control stray flux. In contrast control-based methods have primarily been considered to mitigate crosstalk in electrostatic systems, including feedback control [10] and input-shaping techniques [11,12]. Piezoelectric scanners also often employ structural decoupling techniques, such as hybrid actuation schemes to physically block the transfer of mechanical stress between axes [7].

However, these strategies have their own limitations. Structural mitigation often introduces design constraints,

*These authors contributed equally to this work.
+Corresponding author: jcho@keti.re.kr
Received : Oct. 19, 2025, Revised : Oct. 28, 2025, Accepted : Nov. 4, 2025

increases device size and fabrication complexity, and leads to a lack of design flexibility after fabrication. On the other hand, previously reported control-based solutions involve different challenges. For example, feedback control is inherently limited by loop delay and settling time, which makes it less effective for suppressing high-frequency crosstalk [10]. Other methods such as input shaping [11,12] can significantly increase the computational load required for real-time control. Consequently, both approaches can be challenging for resource-constrained applications, either by increasing hardware complexity or computational demand.

To overcome these limitations, we propose a feedforward control for an electromagnetic 2-axis MEMS that uses a countersignal to suppress the effect of magnetic field coupling. The countersignal is designed as a gain-scaled, phase-inverted replica of the input signal of the counterpart axis to cancel crosstalk. This approach can suppress high-frequency crosstalk effectively without a need for feedback loop control or complex computational resources. The proposed method is data-driven because it is based on experimentally acquired system data, it can also be implemented in a resource-efficient manner with FPGA hardware. Thus, our approach offers a practical and scalable solution to control compact MEMS mirror systems.

The remainder of this study is organized as follows. In Section II, we analyze the characteristics of 2D MEMS mirrors and the mechanisms of crosstalk generation. In Section III, we present the proposed feedforward control system, and we discuss the details of the FPGA implementation as well as the experimental results in Section IV. Finally, we conclude in Section V by summarizing our findings and suggest some possible directions for future research.

2. CHARACTERISTICS OF A 2D MEMS

2.1 Basic Structure and Operation

Fig. 1 shows the electromagnetic actuation-type 2D MEMS mirror considered in this work. The device consists of two driving coils arranged around a mirror plate and permanent magnets placed beneath the substrate [13]. Lorentz forces are generated when a current flows through the coils, which induces a rotational motion of the mirror about two orthogonal axes. The current applied to the outer coil (blue line) rotates the mirror about the y-axis, which causes a laser beam incident at the mirror to be deflected along the horizontal (x-axis) direction. Conversely, the current applied to the inner coil (red line) rotates the mirror about the x-axis and deflects the beam along the vertical (y-axis) direction. This coil-axis mapping enables independent control of horizontal and vertical beam

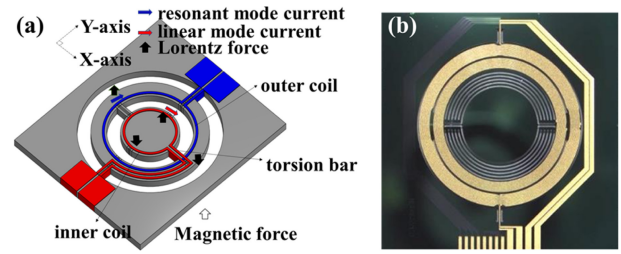

Fig. 1. 2D MEMS (a) Illustration and (b) Photograph.

deflection.

To perform a raster scan using the MEMS mirror, the mirror must scan rapidly along the horizontal direction while moving slowly in the vertical direction [8]. To achieve this, the x-axis is driven in a resonant mode with a sinusoidal current at the mirror's resonant frequency for fast horizontal scanning. Meanwhile, the y-axis is driven in a linear mode with a low-frequency current, and the rotation angle of the mirror varies linearly with the driving current to produce slow vertical motion.

To accurately monitor and control the raster scan, the MEMS mirror consists of two piezoresistive sensors [14] embedded in each torsion bar, which convert the mechanical stress caused by the deflection of the mirror into resistance variations. This piezoresistive sensor produces an electrical voltage as a position signal and enables an accurate estimation of the optical deflection angle with high linearity between the resistance change and the deflection angle [15,16].

2.2 Cross-axis Coupling of 2D MEMS

In electromagnetic 2-axis MEMS, **cross-axis coupling** (also called crosstalk) refers to mutual interference between orthogonal axes caused by electromagnetic coupling. In general, crosstalk is observed on the relatively slow linear (non-resonant) drive axis, and is caused by the dynamic coupling of the high-speed resonant drive axis [17].

Fig. 2(a) illustrates an ideal scan line (black) and a real scan line (red dashed line), which is affected by crosstalk. The scan line exhibits an angular deviation from the ideal horizontal trajectory

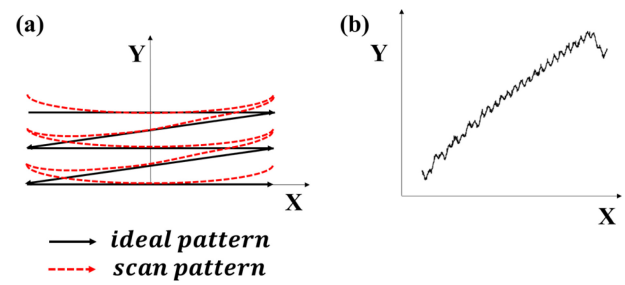

Fig. 2. Effects of crosstalk (a) Angular deviation in Raster scan and (b) Distortion of Position signal

and forms a diagonal pattern on the observation surface.

Here, the position signal from the piezoresistive sensor in the electromagnetic MEMS also exhibits deviation due to crosstalk, as shown in Fig. 2(b). This type of error in the position signal is particularly challenging because it contains high-frequency components induced by a resonantly driven axis. Given that these error components often occur at frequencies far exceeding the control bandwidth of a typical feedback loop, which is inherently limited by latency and settling time, feedback-based compensation becomes ineffective [10]. A feedback controller simply cannot react sufficiently quickly to measure and correct such rapid, high-frequency disturbances. This highlights the need for an alternative approach.

3. COUNTERSIGNAL DESIGN

The MEMS scanner with cross-axis coupling is modeled [F] as a 2 × 2 transfer function matrix as given below.

$$\begin{bmatrix} X_{out} \\ Y_{out} \end{bmatrix} = \begin{bmatrix} H_{xx} & H_{yz} \\ H_{xy} & H_{yy} \end{bmatrix} \begin{bmatrix} X_{in} \\ Y_{in} \end{bmatrix}, \quad (1)$$

where X_{in} and Y_{in} denote the input signals applied along the x- and y-axes, respectively. H_{xx} and H_{yy} represent the single-input single-output transfer functions of the x- and y-axes, respectively, and X_{out} and Y_{out} correspond to the system outputs (i.e., the optical deflection angle from the piezoresistive sensor). The terms $H_{xy} \cdot X_{in}$ capture the crosstalk component induced on the y axis by the resonant mode input X_{in}. Because the crosstalk predominantly appears in the linear mode axis, the countersignal design focuses only on the y-axis.

To compensate for this coupling term, the countersignal for the y-axis is designed as

$$Y_{in}^{count} = Y_{in} + \alpha \quad (2)$$

where Y_{in}^{count} denote the countersignal applied to the y-axis and α represents an additional term to suppress crosstalk. When this countersignal defined in (2) is applied Eq. (1), the y-axis output becomes

$$Y_{out} = H_{yy} \cdot Y_{in} + H_{yy} \cdot \alpha + H_{xy} \cdot X_{in} \quad (3)$$

To eliminate the crosstalk term, α should be

$$\alpha = -\frac{H_{xy}}{H_{yy}} X_{in} \quad (4)$$

Consequently, countersignal in Eq. (2) can be expressed as

$$Y_{in}^{count} = Y_{in} - \frac{H_{xy}}{H_{yy}} X_{in}. \quad (5)$$

The ratio H_{xy}/H_{yy} can be approximated as a frequency-domain function evaluated at f_r because the resonant x-axis input contains only the resonant frequency component f_r. Thus, the counter-signal can be rewritten as

$$Y_{in}^{count} = Y_{in} - \frac{|H_{xy}(f_r)|}{|H_{xy}(f_r)|} e^{j(\angle H_{xy}(f_r) - \angle H_{yy}(f_r))} X_{in} \quad (6)$$

where $|H_{ij}|$ and $\angle H_{ij}$ represent the magnitude and phase of the system gain from input j to output i, respectively.

The numerical values of the countersignal parameters defined in Eq. (6) were obtained from an experimental characterization of the gain of the system in which each axis of the 2D MEMS device shown in Fig. 1 was driven independently using an arbitrary function generator. To isolate each system gain under sinusoidal excitation, a sinusoidal input was applied to one axis while the other axis was grounded.

The measured magnitudes and phases of H_{xy} and H_{yy} are represented in Fig. 3. Fig. 3(a) shows the waveforms of $Y_{in} \cdot H_{yy}$ (red) and $X_{in} \cdot H_{xy}$ (green), which are both obtained on the y-axis when the same sinusoidal input signal was applied to the y- and x-axis, respectively. To analyze their characteristics in the

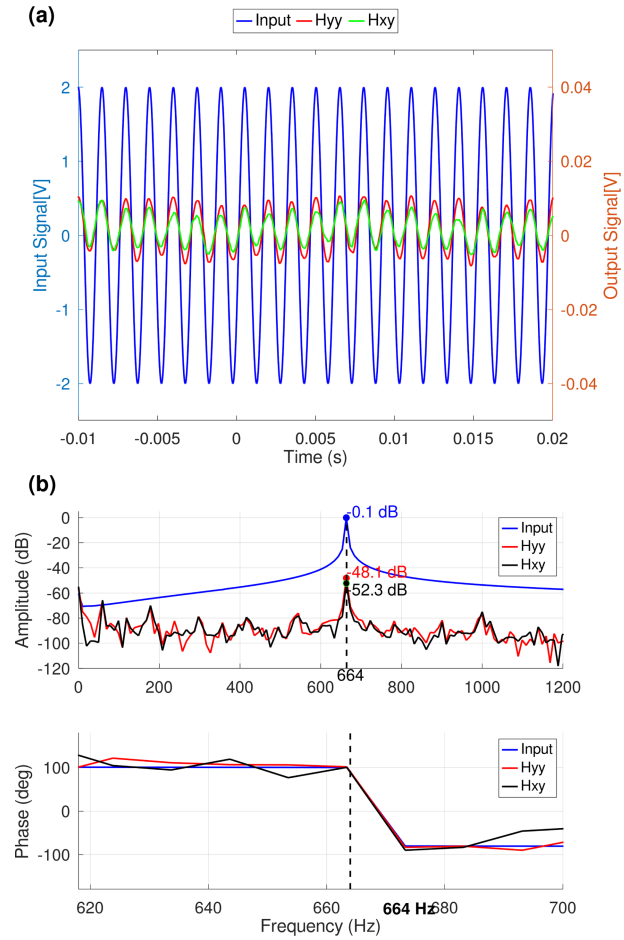

Fig. 3. Transfer function of 2D MEMS (a) Waveforms, and (b) FFT results.

Table 1. Gain and phase delay of transfer function.

	H_{xy}	H_{yy}
$\lvert H(f_r)\rvert$	−52.3dB	-48.1dB
$\angle H(f_r)$	0.3°	0.9°

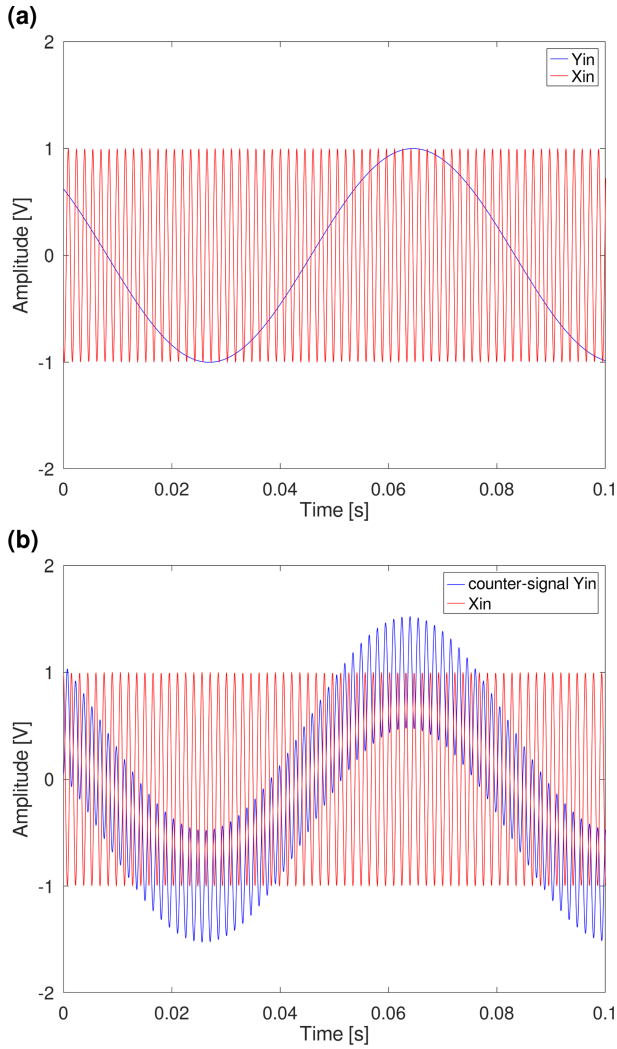

Fig. 4. 2D MEMS input signal (a) Baseline input, and (b) Countersignal input.

frequency domain, their dynamic response was analyzed via a fast Fourier transform (FFT) as shown in Fig. 3(b). The amplitude and phase of H_{yy} and H_{xy} at the resonant frequencies were recorded as -48.1 dB and -52.3 dB, and 0.9° and 0.3°, respectively. As a result, we obtained optimal values for the countersignal to minimize the effects of crosstalk, which are summarized in Table 1.

As shown in Table 1, at the resonant frequency (664 Hz), the magnitudes were H_{xy} = −52.3 dB and H_{yy} = −48.1 dB, corresponding to a gain ratio of -4.2 dB. The measured phase angles were 0.3° and 0.9°, which indicates that the phase difference between H_{xy} and H_{yy} was negligible.

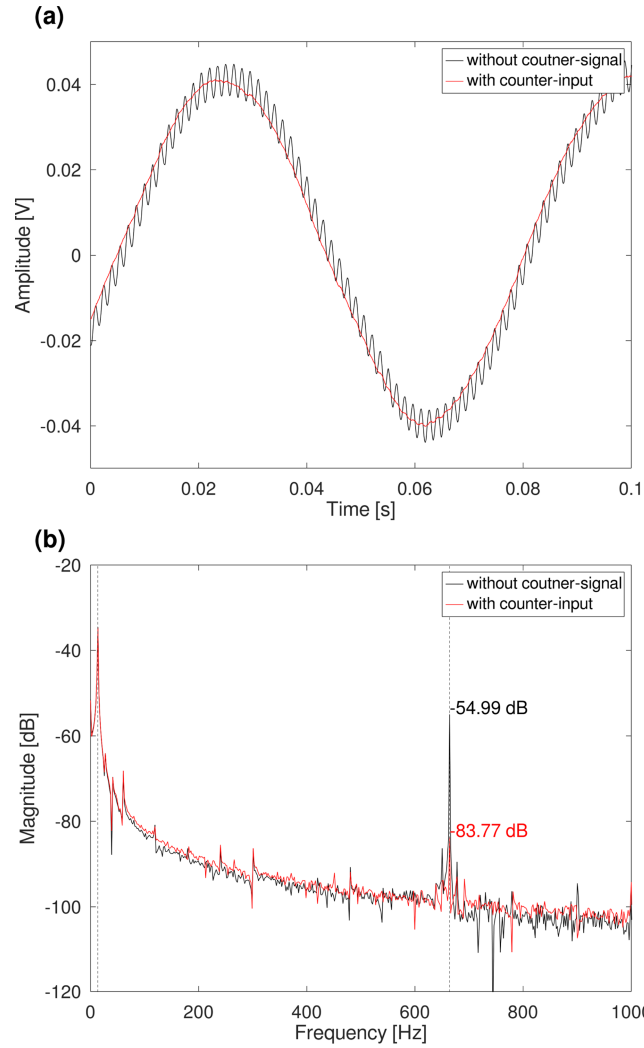

Fig. 5. 2D MEMS output signal (a) Waveforms, and (b) FFT results.

Fig. 4(a) shows the baseline input in time domain when 664 Hz and 13.4 Hz sinusoids were simultaneously applied to the x- (red) and y-axes (blue), respectively. Based on this baseline signal, the countersignal input was generated using (5) and the parameter values in Table 1, as shown in Fig. 4(b). The gain difference of −4.2 dB corresponds to a voltage amplitude ratio of approximately 0.61. The countersignal includes an additional x-axis excitation scaled by 0.61 and phase-inverted by 180 ° superimposed on the y-axis input to minimize x-axis–induced crosstalk. Fig. 5(a) shows the measured output position signal of the 2D MEMS under the baseline input (black) and countersignal (red), respectively. To address output linearity, the dynamic response was analyzed using an FFT as shown in Fig. 5(b). The amplitude of the crosstalk, −54.99 dB with the baseline input, was lowered by -83.77 dB using the countersignal input.

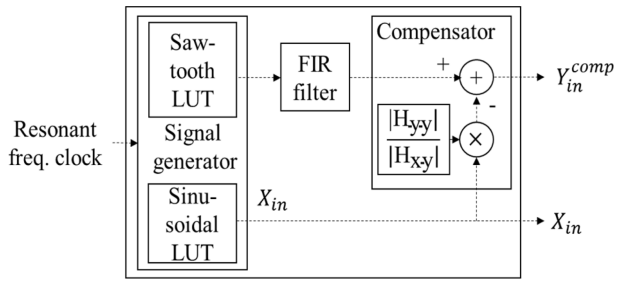

Fig. 6. Block diagram of the feedforward control system.

4. EXPERIMENT AND RESULT

4.1 Implementation and Experimental setup

The proposed feedforward control system was implemented on FPGA logic. As shown in Fig. 6, the control system consisted of a sawtooth lookup table (LUT), a direct digital synthesizer (DDS)-based sinusoidal LUT, and several digital operators, such as adders and multipliers. Specifically, a feedforward term of the y-axis proportional to the x-axis input scaled by $|H_{xy}(f_r)|/|H_{yy}(f_r)|$ and phase-shifted by 180° was added to the output of the sawtooth LUT to cancel out the crosstalk. To suppress high-frequency harmonics, a finite impulse response (FIR) filter was placed downstream of the sawtooth function LUT. The FIR filter was designed with 2047 taps and a cutoff frequency of 270 Hz, which corresponds to the resonant frequency of the linear axis.

We used the experimental setup shown in Figs. 7 and 8 to evaluate the proposed feedforward control system. The specifications of the experimental setup are summarized in Table 2. It consisted of a Xilinx Zynq FPGA platform, a 2D MEMS, and its driver circuit. The main components of the driver circuit included a programmable oscillator, 16-bit analog-to-digital (ADC) and digital-to-analog converters (DAC). The control signals of the ADC and DAC were generated by an FPGA and applied through a serial peripheral interface (SPI). The programmable oscillator provides a resonant-frequency clock to the FPGA, in which the DDS

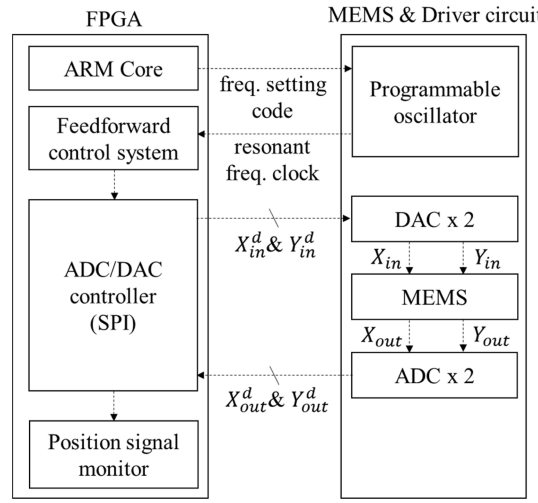

Fig. 7. Schematic diagram of the experimental setup.

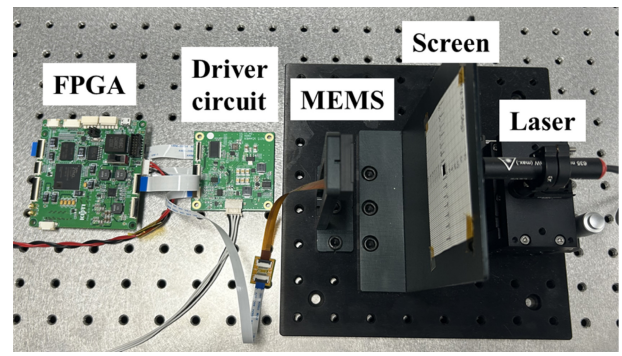

Fig. 8. Photograph of the experimental setup.

LUT and sawtooth LUT generate sinusoidal and sawtooth driving signals corresponding to the x- and y-axes, respectively. When the input driving signals are applied to the driver circuit, they are converted into analog voltages by the DAC and applied to the MEMS mirror. Meanwhile, the position signals produced in the 2D MEMS are converted into digital signals by the ADC and applied to the position signal monitoring block in the FPGA. To observe the scanning pattern, a testbench consisting of a laser and a screen was also constructed as shown in Fig. 8.

Table 2. Experiment setup specification

Component	Specification
FPGA	Xilinx Zynq-7020
ADC	16 bits resolution, 1MSPS, SPI interface
DAC	16 bits resolution, 250kSPS, SPI interface
MEMS	Electromagnetic 2D MEMS (Ø5 mm mirror) Resonant axis @ 644Hz, linear axis @ 13.3Hz

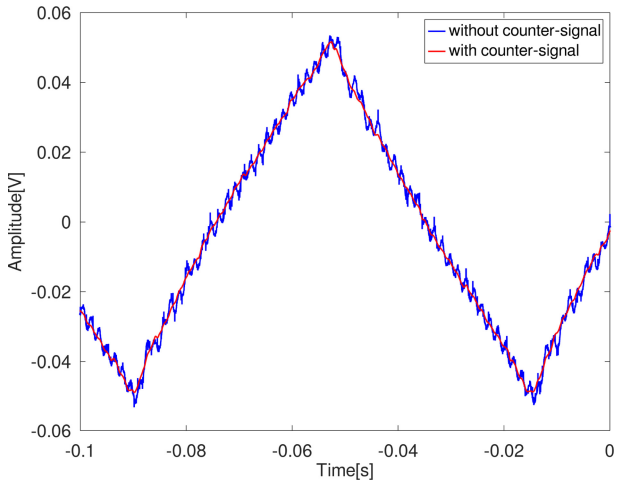

Fig. 9. Position output with and without counter-signal.

Table 3. FPGA resource utilization.

Resource	Without c-.s	With c-.s
LUT	13965	13981
Flip-Flop	24051	24052
BRAM	30.5	30.5
DSP	165	165

4.2 Experimental Results

Fig. 9 shows the optical deflection results as observed from the position signal of the linear mode axis when applying the proposed feedforward control. Comparing the results with the baseline input, the linear scan pattern demonstrated improved linearity of the mirror motion when the crosstalk-cancellation signal was applied. To quantitatively evaluate the degree of improvement in linearity, several numerical measures were examined and a slope analysis was performed as described in the following subsections.

FPGA resource utilization was analyzed to confirm the efficiency of the hardware used to implement the proposed countersignal control. Table 3 shows that countersignal control was achieved with relatively limited additional usage of logic resources such as LUTs, flip-flops (FFs), block RAMs (BRAMs), and digital signal processing (DSP) slices.

4.2.1 Quantitative Evaluation of Linear Actuation

The linear actuation performance of the MEMS mirror was evaluated within an input range of 10 to 90% of the full scan. Linear interpolation was applied to this range, and the error was defined as the difference between the signal and a line. A smaller error indicates a more uniform optical scanning speed.

Table 4. Linear actuation performance.

Range	Metric	Without c-.s	With c-.s
[10%, 90%].	RMS Error	2.2e-3	1.3e-3
	Max Error	7.3e-3	3.5e-3
	R^2	0.991	0.996
[20%, 80%].	RMS Error	2.0e-3	0.6e-3
	Max Error	5.9e-3	1.4e-3
	R^2	0.987	0.999

Measures of linearity including the coefficient of determination (R^2), root-mean-square error (RMS), and maximum error (Max) were calculated using the datasets of the position output with and without countersignals.

As summarized in Table 4, the RMS and maximum errors were significantly reduced after applying the feedforward control, with the coefficient of determination (R^2) approaching unity in both ranges. These results confirm that the proposed feedforward control effectively enhanced the linearity and uniformity of optical scanning motion of the mirror. After control, the R^2 value reached 0.996, which confirms that the linearity requirement of above 0.995 for scanning using a MEMS mirror was satisfied [18].

4.2.2 Slope Consistency Analysis

The variability and standard deviation of the slope of each scan were calculated to quantitatively compare the scanning quality. The slope of the mirror deflection was computed by differentiating the position output with and without countersignals over the range [10-90%]. The standard deviation (STD) and coefficient of variation (CV) were calculated to quantify the consistency of the slope.

The deviation in the position output without a countersignal (blue) and with countersignal (red) deflection signals over the rising range [10-90%] is illustrated in Fig. 10. For the position output without a countersignal, the standard deviation was 7.8 and the coefficient of variation was 243, which indicates large fluctuations around the mean slope. For the position output without a countersignal, the standard deviation decreased to 1.5 and CV to 59, which shows that fluctuations in the slope were significantly suppressed. The position output with the countersignal exhibited a smaller deviation around the mean slope, which is consistent with the quantitative reduction in CV shown in Table 5.

The lower CV and standard deviation after control confirmed that the slope of the deflection signal remained more consistent, which demonstrates that the proposed feedforward method improved the linearity and uniformity of the scanning process performed with the MEMS mirror.

Table 5. Standard deviation and coefficient of variation of position outputs.

Metric	Without c-.s	With c-.s
STD	7.8	1.5
CV	243	59

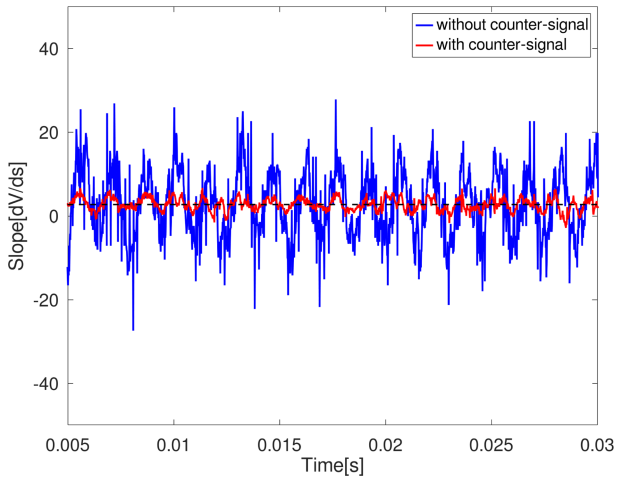

Fig. 10. Deviation of slope of position output

5. CONCLUSIONS

In this study, we have proposed a digital feedforward control framework that employs a countersignal to suppress the effects of high frequencies in an electromagnetic 2D MEMS mirror during raster scanning. The proposed control system synthesizes a countersignal by applying a proportional and opposite phase to the counterpart input, which is derived from experimentally obtained transfer-function gains at the resonant frequency of the 2D MEMS mirror. Owing to the simplicity of the proposed approach, the system is implemented on an FPGA without any complex computation procedures or full-spectrum modeling.

The feasibility of the method was validated using an experimental setup comprising an FPGA platform, a 2D MEMS, and a driver circuit, and the results demonstrated significant improvements in the linearity of the motion of the mirror. Specifically, the RMS and maximum errors of the linear axis were reduced by 38% and 49%, respectively, while the coefficient of determination (R^2) increased from 0.991 to 0.996. Moreover, the coefficient of variation (CV) of the slope decreased from 243% to 59%, which confirms that our method exhibited enhanced scanning uniformity.

In summary, the proposed method provides a practical and computationally efficient solution to suppress crosstalk in real time in compact MEMS mirror control systems. However, it is important to note that our feedforward approach and a conventional feedback system target different control objectives. The proposed feedforward method is specifically designed to suppress high-frequency crosstalk originating from the fast resonant axis, which is a challenge for feedback systems due to inherent limitations in loop delay. In contrast, feedback control is generally effective for correcting low-frequency nonlinearities and drift. In terms of hardware resources, our feedforward technique can be implemented by adding relatively few LUT and flip-flop blocks. A feedback system capable of addressing similar high-frequency phenomena would require a significantly more complex architecture, including high-speed ADCs and a low-latency processing pipeline, which would lead to substantially higher resource consumption.

The proposed digital feedforward architecture can be readily adapted to different MEMS devices or structural variations simply by updating the experimentally measured system parameters, which can ensure robustness to fabrication and resonance variations. These results demonstrate the strong potential of our proposed method for LiDAR applications in which precise and uniform scanning performance is critical. In future research, a hybrid control scheme could combine this feedforward method with feedback control to suppress both high-frequency crosstalk and low-frequency drift to further improve linearity.

CRediT Authorship Contribution Statement

Sang-gyun Gi: Conceptualization, Project administration, Resources, Supervision, Writing – review and editing. **Sehwan Park:** Conceptualization, Methodology, Data curation, Formal analysis, Validation, Investigation, Software, Visualization, Resources, Writing – original draft. **Junseop Lee:** Supervision **Seungjoo Lee:** Funding acquisition, Project administration, Supervision. **Jihyuk Cho:** Project administration, Supervision.

Declaration of Competing Interest

The authors declare that they have no known competing financial interests or personal relationships that could have appeared to influence the work reported in this paper.

Acknowledgements

S.G. and S.P. contributed equally to this work. This work was supported by the Technology Innovation Program (RS-2023-00234343, Development of key photonic components and micro photonic integrated circuit module to commercialize high-resolution 4D FMCW MEMS LiDAR for autonomous vehicles) funded by the Ministry of Trade, Industry and Energy (MOTIE, Korea) and Korea Planning & Evaluation Institute of Industrial Technology (KEIT).

REFERENCES

[1] V. Milanović, A. Kasturi, J. Yang, F. Hu, Closed-loop control of gimbal-less MEMS mirrors for increased bandwidth in LiDAR applications, Proceedings of the SPIE Conference on Laser Radar Technology and Applications XXII, Anaheim, USA, 2017, pp. 1–13.

[2] R. Schroedter, M. Roth, K. Janschek, T. Sandner, Flatness-based open-loop and closed-loop control for electrostatic quasi-static microscanners using jerk-limited trajectory design, Mechatronics 56 (2018) 318–331.

[3] H. Urey, S. Holmstrom, U. Baran, MEMS laser scanners: a review, J. Microelectromech. Syst. 23 (2014) 259–275.

[4] A.R. Cho, A. Han, S. Ju, H. Jeong, J.H. Park, I. Kim, et al., Electromagnetic biaxial microscanner with mechanical amplification at resonance, Opt. Express 23 (2015) 16792–16802.

[5] K. Kim, S. Moon, J. Kim, Y. Park, J.H. Lee, Two-axis crosstalk analysis of gimbal-less MEMS scanners with consideration of rotational alignment, Measurement 171 (2021) 108785.

[6] J. Žumer, D. Reynaerts, M. Boltežar, An advanced nonlinear model of a low-g MEMS accelerometer for a computer pen, Measurement 45 (2012) 459–468.

[7] H. Li, J. Hou, Z. Gong, H. Yu, Y. Liu, W. Shen, Hybrid actuation MEMS micromirror with decoupled piezoelectric fast axis and electromagnetic slow axis for crosstalk suppression, Micromachines 16 (2025) 1072.

[8] Y.K. Yong, K. Liu, S.O.R. Moheimani, Reducing cross-coupling in a compliant XY nanopositioner for fast and accurate raster scanning, IEEE Trans. Control Syst. Technol. 18 (2010) 1172–1179.

[9] S.Y. Kang, J.-H. Park, C.-H. Ji, Design optimization of a 6.4 mm-diameter electromagnetic 2D scanning micromirror, Opt. Express 28 (2020) 31272–31286.

[10] H. Chen, A. Chen, W.J. Sun, Z.D. Sun, J.T. Yeow, Closed-loop control of a 2-D MEMS micromirror with sidewall electrodes for a laser scanning microscope system, Int. J. Optomechatronics 10 (2015) 1–13.

[11] K. Kim, J. Kim, Y. Park, S.-H. Kim, J.-H. Lee, Shaped input for reducing crosstalk of two-axis MEMS scanners, Sens. Actuators A Phys. 349 (2023) 114002.

[12] A. Li, H. Huang, P. Zhang, Y. Su, Y. Zhang, L. Wang, et al., Determination of crosstalk in a dual-axis piezoelectric MEMS mirror and suppression with feedforward algorithms, IEEE Sensors J. 24 (2024) 32272–32282.

[13] A. Setiarini, G. Sugandi, Y.N. Wijayanto, G. Wiranto, R.V. Manurung, I.D.P. Hermida, A novel structure of electromagnetic MEMS speaker for hearing aid application, Proceedings of the 2018 International Conference on Radar, Antenna, Microwave, Electronics, and Telecommunications (ICRAMET), Serpong, Indonesia, 2018, pp. 112–116.

[14] P. Frigerio, R. Carminati, L. Molinari, G. Langfelder, Piezoresistive versus piezoelectric position sensing in MEMS micromirrors: A noise and temperature drift comparison, IEEE Sens. Lett. 6 (2022) 1–4.

[15] H. Yu, P. Zhou, K. Wang, Y. Huang, W. Shen, Optimization of MOEMS projection module performance with enhanced piezoresistive sensitivity, Micromachines 11 (2020) 651.

[16] C. Zhang, Z. You, H. Huang, G. Li, Study on a two-dimensional scanning micro-mirror and its application in a MOEMS target detector, Sensors 10 (2010) 6848–6860.

[17] V.D. Ching-Roa, C.Z. Huang, M.G. Giacomelli, Suppression of subpixel jitter in resonant scanning systems with phase-locked sampling, IEEE Trans. Med. Imaging 43 (2024) 2159–2168.

[18] M. Li, L. Qin, X. Wang, J. Wen, T. Wu, X. Huang, et al., The design and performance evaluation of an eye-tracking system based on an electrostatic MEMS scanning mirror, Micromachines 16 (2025) 640.